

Global memory analysis in observed and simulated CAPE and CIN

Kathrin Riemann-Campe,^{a,b*} Richard Blender^b and Klaus Fraedrich^b

^a International Max Planck Research School on Earth System Modelling, Bundesstrasse 53, D-20146 Hamburg, Germany

^b Meteorologisches Institut der Universität Hamburg, Grindelberg 5, D-20144 Hamburg, Germany

ABSTRACT: The memory of convective precipitation is estimated via the analysis of the convective parameters convective available potential energy (CAPE) and convective inhibition (CIN). The variability of mixed layer (ML) CAPE and CIN in present-day climate is presented in terms of a linear decay time scale for short-term memory and the Hurst exponent for long-term memory (determined by detrended fluctuation analysis). Regional and global memory in CAPE and CIN is compared between observations (ECMWF re-analysis, in 1979–2001) and simulated data (ECHAM5/MPIOM, 20C simulation, in 1900–2001). Both datasets agree on the memory pattern in CAPE and CIN with highest values of the Hurst exponent along the equatorial Pacific which decrease towards higher latitudes; however, longest memory up to decades is found in CAPE south-east of Greenland. The memory in CIN is weaker than in CAPE regarding strength and spatial extent. To determine the origin of memory in CAPE and CIN, ML temperature and specific humidity, enthalpy, and latent heat equivalent of precipitable water (LPW) are analysed. In the tropics the spatial characteristics of the memory in CAPE coincide with memory in LPW, while in the extra-tropics ML temperature and humidity have the strongest impact. Copyright © 2010 Royal Meteorological Society

KEY WORDS CAPE; CIN; low frequency variability; persistency

Received 9 July 2009; Revised 23 February 2010; Accepted 8 March 2010

1. Introduction

Memory can be defined as the dependency of a time series value on previous values of the same time series, thus memory is indispensable for prediction. Here, the memory of convective precipitation is analysed, which is relevant for short term and long range prediction. On long time scales convection anomalies affect wetness and droughts, on short time scales severe weather events are relevant for forecasting. As convective precipitation requires parameterisation in numerical models, convective available potential energy (CAPE) and convective inhibition (CIN) are applied to estimate the memory of convective precipitation.

CAPE denotes the potential energy available to form cumulus convection which leads to convective precipitation. The energy is characterised by a positive virtual temperature difference between an idealised rising air parcel and its environment. On the other hand, CIN denotes the energy needed by the parcel to overcome the boundary layer to reach the CAPE above. Therefore, high values of CAPE do not necessarily lead to convection, if the ascent of air is prevented by a stable boundary layer indicated by also high values of CIN. The analysis of energy available for convection reaches back

to Margules (1905). However, the variable CAPE was apparently first mentioned in a publication by Moncrieff and Miller (1976). Since then CAPE and CIN have been used for severe weather analysis and forecasting (e.g. Colby, 1984; Rasmussen and Blanchard, 1998; Craven *et al.*, 2002; Markowski *et al.*, 2002; Brooks *et al.*, 2003, 2007; Doswell and Evans, 2003). CAPE is also used in cumulus parameterisation in general circulation models (e.g. Moncrieff and Miller, 1976; Ye *et al.*, 1998; Washington and Parkinson, 2005). Recent analyses focus on CAPE and its change regarding a warmer climate (Trapp *et al.*, 2007, 2009). Yano *et al.* (2001) are the first to analyse CAPE with respect to memory, reporting 1/f scaling over the tropical western Pacific. Riemann-Campe *et al.* (2009) report indications of low frequency variability in CAPE and CIN over tropical and extra-tropical regions. In general, analyses of inter-annual and inter-decadal memory are widely applied on temperature and moisture variables revealing memory pattern over oceans and continents on almost all latitudes (e.g. Fraedrich and Larnder, 1993; Blender and Fraedrich, 2003; Fraedrich and Blender, 2003; Fraedrich *et al.*, 2004). As CAPE and CIN are variables dependent on temperature and moisture, we expect to find memory signals in these variables too. In addition to CAPE and CIN, temperature and specific humidity in the lowest 100 hPa as well as above are analysed to compare their global memory patterns with those of CAPE and CIN.

* Correspondence to: Kathrin Riemann-Campe, Meteorologisches Institut der Universität Hamburg, Grindelberg 5, D-20144 Hamburg, Germany. E-mail: kathrin.riemann@zmaw.de

Here, we focus on the memory of CAPE and CIN on intra- and inter-annual time scales. Global analysis of a decay time scale (short-term memory, STM) and detrended fluctuation analysis (DFA) (LTM), are applied to observed (ECMWF re-analysis, ERA-40, 1979–2001) and simulated data. The present-day climate is simulated by the Max Planck Institute for Meteorology coupled atmosphere-ocean model (ECHAM5/MPIOM, 1900–2001, simulation 20C). In addition, autocorrelations, power spectra and DFA are applied to regional time series of the above mentioned datasets.

The outline of the paper is as follows: the data and variables are described in detail in Section 2. Section 3 introduces the different kind of methods which are applied here to analyse memory. The findings of regional memory are shown in Section 4, while results on a global scale are shown in Section 5. In Section 6, correlations between CAPE and large-scale atmospheric phenomena indicate possible influences on CAPE variability. Sections 7 and 8 present a discussion and conclusions of the results.

2. Data and variables

In this study daily re-analysis data of the European Centre for Medium-Range Weather Forecast ECMWF (ERA-40) are used in the spectral truncation T106 (horizontal resolution $\sim 1.125^\circ$). Vyushin and Kushner (2009) report an artificial memory signal in temperature over the Southern Ocean in the ERA-40 data due to measuring problems prior 1979. According to Bengtsson *et al.* (2004) and Simmons *et al.* (2004) the ERA-40 data consists of artificial warming trends due to changes within the measurement system prior to 1979. Such trends, independent of their origin, might influence memory signals (Maraun *et al.*, 2004). Therefore, the analysis of the ERA-40 data is restricted to 1979–2001.

The ERA-40 data is compared with a 20th century ensemble simulation (20C) with the coupled atmosphere-ocean model ECHAM5/MPIOM (Roeckner *et al.*, 2003), which is a part of the Intergovernmental Panel on Climate Change (IPCC) contributions. The 20C simulation incorporates anthropogenic forcings such as CO₂, CH₄, N₂O, CFCs, O₃ and sulphate and is simulated with T63 spectral truncation ($\sim 1.875^\circ$ resolution) during 1900–2001. For a direct comparison of CAPE and CIN from the simulated data with those computed from the ERA-40 data, the 20C simulation is analysed in the same time period, 1979–2001. Because the memory properties during 1900–2001 are similar to those in the short period (1979–2001), the long period is used for further analysis, for example, for an analysis of El Niño Southern Oscillation (ENSO), which is expected to influence the memory of CAPE in the tropics.

2.1. CAPE and CIN

CAPE describes the potential energy available to be transformed into kinetic energy to develop cumulus

clouds. This energy is calculated by comparing the virtual temperature profile of the atmosphere to the virtual temperature of an idealized rising air parcel. The parcel starts from the top of an assumed ML, which covers the lowest 100 hPa of the atmosphere. The parcel follows a dry adiabatic ascent until the lifting condensation level (LCL) is reached. From the LCL the parcel follows a moist adiabat; condensing moisture within the parcel is assumed to fall out immediately as rain. CAPE is defined between the level of free convection (LFC) and the level of neutral buoyancy. Between these levels the virtual temperature of the parcel T_{vp} is higher than the virtual temperature of the atmosphere T_{ve} . Thus, the density in the parcel is lower than its surrounding air, which leads to an ascent, hence:

$$\text{CAPE} = \int_{\text{LFC}}^{\text{LNB}} R_d (T_{vp} - T_{ve}) d \ln(p), \quad (1)$$

where R_d denotes the gas constant of dry air and p is pressure (Emanuel, 1994).

CIN describes the convective energy needed by the rising parcel to overcome the boundary layer to reach the LFC:

$$\text{CIN} = \int_{\text{ML}}^{\text{LFC}} R_d (T_{ve} - T_{vp}) d \ln(p). \quad (2)$$

The assumed ML over the lowest 100 hPa is also considered in the calculation of CIN. As the parcel starts its ascent from the top of the ML, CIN is computed only between the ML and the LFC.

CAPE and CIN depend on temperature and humidity, so the memory signals of CAPE and CIN are compared to those of the mean values of temperature T_{ML} and specific humidity q_{ML} within the ML, and to the mean values of temperature and specific humidity between the ML and the 100 hPa level.

For a consistent comparison, temperature and specific humidity above the ML are converted to energy. The temperature is multiplied by the heat capacity of dry air at constant pressure c_p with individual values at each pressure level p_k , $k = \text{ML}, \dots, 100 \text{ hPa}$ yielding enthalpy H with the same units as CAPE and CIN, [H] = J/kg:

$$H = \frac{1}{n_L} \sum_{k=\text{ML}}^{100 \text{ hPa}} (c_p T)_k, \quad (3)$$

where n_L denotes the number of vertical levels between the ML and 100 hPa.

For the same reason, specific humidity between the ML and 100 hPa is multiplied by the latent heat of evaporation L (also varying with height). The resulting vertical mean of latent heat equivalent of precipitable water LPW is also counted in units of energy per mass, [LPW] = J/kg:

$$\text{LPW} = \frac{1}{n_L} \sum_{k=\text{ML}}^{100 \text{ hPa}} (Lq)_k. \quad (4)$$

3. Analysing STM and LTM

Memory of meteorological time series may roughly be divided into STM and LTM processes, with a threshold often given by the synoptic time scale. In many circumstances, STM processes are adequately simulated by autoregressive (AR) processes. For example, the memory of a first order, AR(1) can be measured by the finite decay time scale of the exponentially decreasing autocorrelation function (ACF). On longer, say inter-annual time scales many climatological time series may reveal LTM which is related to increasing variance for decreasing or low frequencies; the ACF does not decay exponentially, inhibits the definition of a decay time scale and the power spectrum increases typically according to a power law, $S(f) \sim f^{-\beta}$ with positive exponents $0 < \beta < 1$. In the following STM and LTM are described and methods for analysis are presented.

3.1. STM: decay time scale τ

Autoregressive processes of first order have been used to investigate and estimate memory in climate time series:

$$x_t = \phi x_{t-\Delta t} + \varepsilon_t \quad (5)$$

with autocorrelation coefficient (ACC) ϕ and white noise forcing ε_t . The decay time scale τ is given by $\tau = \Delta t / (1 - \phi)$ with the time step Δt . Trends and periodic components, e.g. diurnal and seasonal cycles need to be removed as previous studies have shown that CAPE and CIN are non-stationary (Riemann-Campe *et al.*, 2009) with trends and annual cycles. Here, the decay time scale is computed for daily and monthly mean values of CAPE and CIN in ERA-40 data and the 20C simulation.

3.2. LTM: DFA

The DFA (DFA, Peng *et al.*, 1995) provides a method to detect LTM in stationary time series which would not be accessible in an ACF or the power spectrum. As a first step the standardised anomalies of a time series are computed by removing the mean annual cycle and dividing by the standard deviation. Then, the profile y_j of the standardised anomalies x_i , $i = 1, \dots, N$, of total length N is computed by $y_j = \sum_{i=1}^j x_i$. The profile is divided into segments of equal length s , which overlap for 50%. In each segment a polynomial \hat{y}_j with degree k is fitted to the profile. The degree of the polynomial used is denoted by the version of the DFA, e.g. DFA2 uses polynomials of the second order. The root mean square error is computed by the deviations in the segments resulting in the fluctuation function $F(s)$

$$F(s) = \sqrt{\frac{1}{N} \sum_j^N (y_j - \hat{y}_j)^2} \quad (6)$$

The fluctuation function is computed repeatedly for varying segment lengths s . For a scaling LTM the fluctuation function is $F(s) \sim s^\alpha$ with the Hurst exponent $\alpha \geq 0.5$, which is related to the power spectral exponent

$\beta = 2\alpha - 1$. In the presence of linear trends, LTM is determined by DFA2 (Maraun *et al.*, 2004) (note that DFA does not remove trends). If oscillations are superimposed on a LTM signal, the scaling of $F(s)$ is interrupted by an increase of variability on the time scale given by the oscillation. This is typically observed as a saddle point (Fraedrich, 2002). The uncertainty of the DFA exponent is $\Delta\alpha \approx 0.05$ and $\Delta\beta \approx 0.1$ (Fraedrich and Blender, 2003). Therefore, memory is recognised here if $\alpha \geq 0.55$.

4. Regional memory

Memory in CAPE and CIN is analysed in greater detail in two regions to investigate the origins of the memory. A first focus is on the western equatorial Pacific (at $\sim 160^\circ\text{E}$, 0.5°N). Yano *et al.* (2001) reported $1/f$ scaling in CAPE in this region. A second region is chosen in the North Atlantic south-east of Greenland (at $\sim 40^\circ\text{W}$, 59°N) where LTM in sea surface temperature (SST) was found by Fraedrich and Blender (2003). Furthermore, Claud *et al.* (2007) reported a relation between North Atlantic Oscillation (NAO) and polar low development which occurs simultaneously with CAPE development. Thus, the NAO is expected to be related to the memory in CAPE. ACF, power spectra, and DFA2 are applied to daily mean values of CAPE and CIN. In addition the fluctuation functions of ML temperature, T_{ML} , and humidity, q_{ML} , H , and LPW are analysed to reveal their relations to CAPE and CIN.

4.1. Western equatorial Pacific

The ACF in Figure 1(a) shows memory on short time scales, up to 50 days. The ACC, is positive for CAPE and CIN from the 20C simulation. Although the ACC is lower in CAPE from ERA-40 data compared to CAPE from the 20C simulation, the slopes of the ACF are similar with increasing lag. In contrast, the short memory in CIN ends after 6 days when computed from ERA-40 data, while it lasts up to 50 days when computed from the 20C simulation. The log-lin diagram, chosen to focus on STM as well as to $1/f$ -like behaviour, shows power laws in CAPE between 1 and 10 days, and nearly constant ACCs between 10 and 20 days. The ACC found in CAPE hints to memory on longer time scales, which cannot be analysed by ACF. Indeed, the power spectra (Figure 2(a)) and DFA2 (Figure 3(a)) reveal memory on longer time scales up to 500 days. This long memory in CAPE is caused by large-scale atmospheric flow conditions favouring CAPE development. Moreover, the power law exponent β is continuously positive for CAPE and CIN with a superimposed cycle between 1000 and 2000 days in the 20C simulation. In contrast, β is positive in CAPE and CIN up to about 1000 days without a superimposed cycle in the ERA-40 data. Although β is mostly positive, its magnitude varies with higher values during the first 10 days. The Hurst exponent α of CAPE and CIN reveals also a superimposed cycle between 1000 and 2000 days

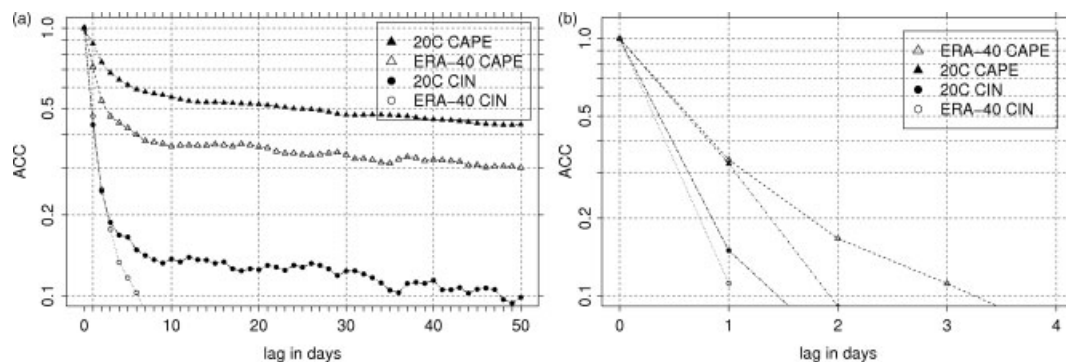


Figure 1. ACF of CAPE (triangle) and CIN (circle) at the equatorial Pacific (a), and south-east of Greenland (b) computed from ERA-40 data (open symbols) and the 20C simulation (filled symbols).

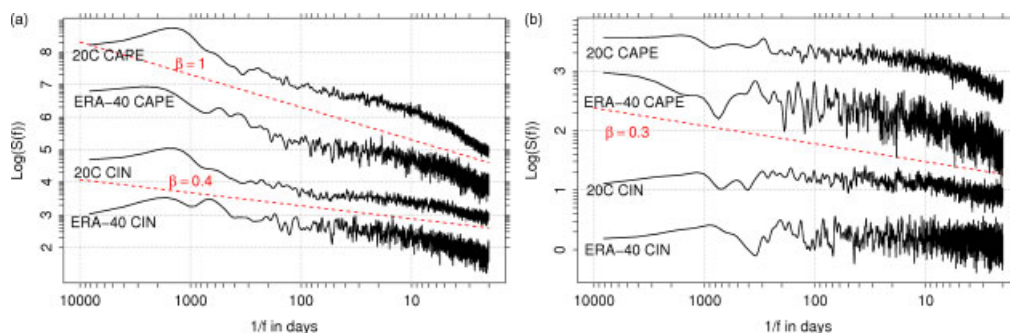


Figure 2. Power spectra of CAPE and CIN at the western equatorial Pacific (a), and south-east of Greenland (b) computed from ERA-40 data (1979–2001) and the 20C simulation (1900–2001). Dashed lines indicate exponents β . Spectra are shifted vertically to avoid overlap. This figure is available in colour online at www.interscience.wiley.com/ijoc

in the 20C simulation (Figure 3(a)). It is not clear whether the enhanced slope around 2000 days in CAPE indicates a cycle in the ERA-40 data. Prior to the occurrence of the cycle the slope α equals approximately one for CAPE and $\alpha \sim 0.7$ for CIN in both datasets. As the cycle is indicated by a ‘saddle point’, the slope increases and decreases, respectively, within the cycle and thus changes the value of α within the considered frequency range. The period of the cycle between 1000 and 2000 days as well as its location suggest ENSO to be the physical mechanism. van Oldenborgh *et al.* (2005) reported that ENSO is realistically represented in the 20C simulation. Moreover, the short time series of the analysed ERA-40 data is not an ideal source to analyse ENSO regarding its strength. The long memory as well as ENSO is also present in T_{ML} , q_{ML} , H , and LPW in the 20C simulation (Figure 3(c) and (e)). While the fluctuation function of T_{ML} , q_{ML} , and LPW resemble that of CAPE with $\alpha \sim 1$, H reveals a second cycle between 60 and 70 days in the ERA-40 data.

4.2. South-East of Greenland

The ACF shows that the short memory in CAPE and CIN lasts only for a couple of days above the North Atlantic (Figure 1(b)). The duration of the memory corresponds to the life span of synoptic disturbances, e.g. polar lows which consist of high magnitudes of CAPE and low values of CIN. However, the power spectra (Figure 2(b)) and fluctuation functions (Figure 3(b)) reveal LTM up

to 9000 days. CAPE and CIN computed in the 20C simulation reveal a uniform slope of $\alpha \sim 0.65$, $\beta \sim 0.3$, respectively, with an exception during the first 10 days in CAPE. In contrast, CIN computed from the ERA-40 data does not reveal any memory. Thus, the question arises why CIN differs in ERA-40 and in the 20C simulation above the North Atlantic but not above the equatorial Pacific. The fluctuation functions of T_{ML} , q_{ML} , H , and LPW reveal also memory up to the total duration of the time series with a relatively uniform $\alpha \sim 0.65$. The long memory visible in CAPE, T_{ML} , q_{ML} , H , and LPW is probably related to the NAO. A positive correlation between the NAO and CAPE is described in Section 6.

5. Global memory patterns

Global distributions of the decay time scale of daily and monthly values, and the Hurst exponent of intra- (30–300 days) and inter-annual (400 days–5 years) periods are obtained from ERA-40 data (1979–2001) and the 20C simulation (1900–2001). Antarctica is not considered in the analysis, because CAPE and CIN values are only computed for approximately 10 days during an average year in this region.

5.1. Intra-annual memory

The global pattern of intra-annual memory is described by the decay time scale of daily, τ_d (Figure 4), and

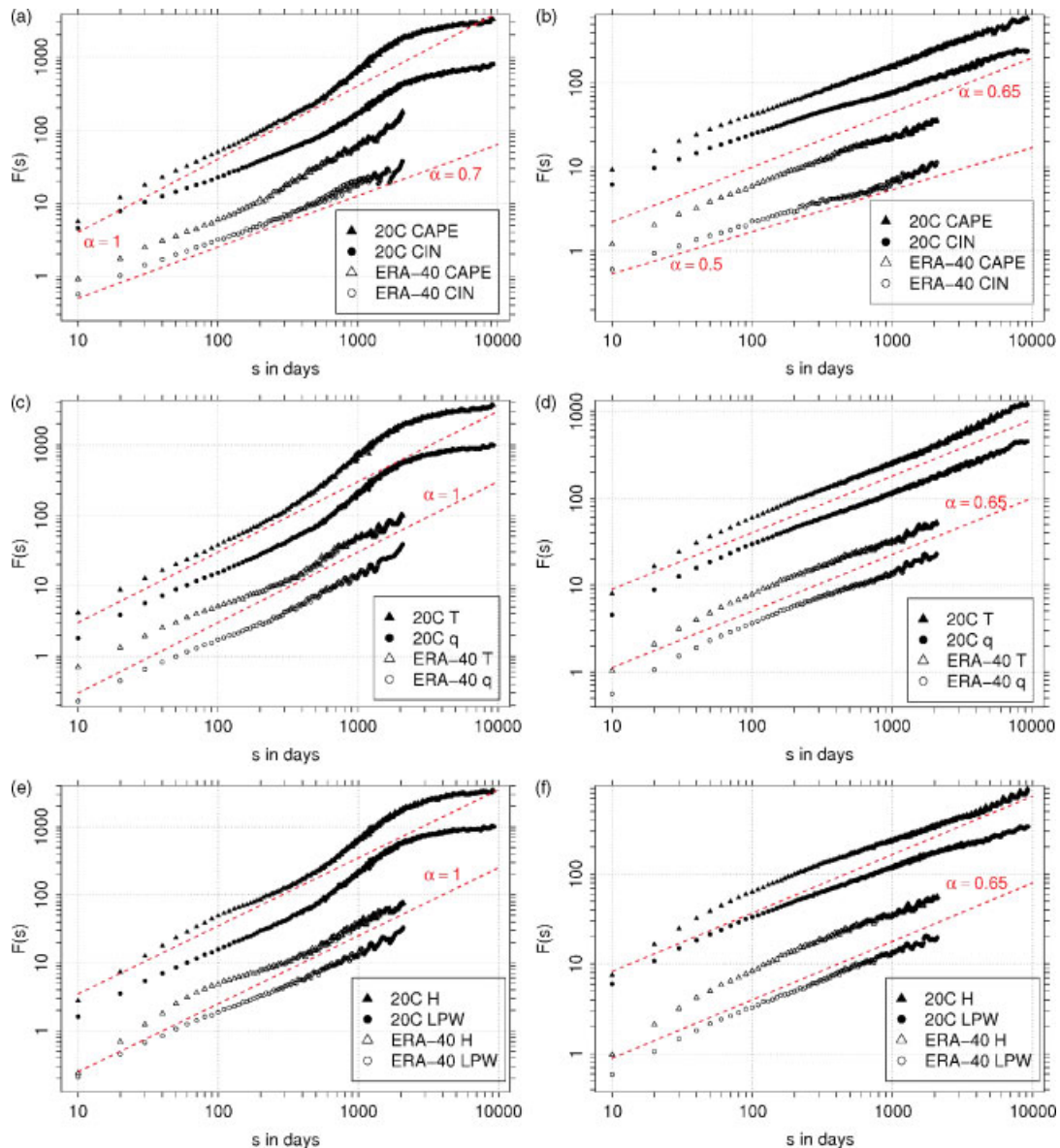


Figure 3. Fluctuation functions (DFA2) at the western equatorial Pacific (a, c, e), and south-east of Greenland (b, d, f) computed from ERA-40 data and the 20C simulation: CAPE and CIN (a and b), ML temperature and specific humidity (c and d), and enthalpy and the latent heat equivalent of precipitable water (e and f). Dashed lines indicate slope α . Fluctuation functions are shifted vertically to avoid overlap. This figure is available in colour online at www.interscience.wiley.com/ijoc

monthly values, τ_m (Figure 5), and the Hurst exponent α in the time interval 30–300 days (Figure 6). All three analyses, τ_d , τ_m , and α , of both data sets agree on the general memory distribution in CAPE. The highest values of τ_d and $\tau_m \geq 5$, and $\alpha \geq 1$ occur along the equatorial Pacific. High values of τ_d , τ_m and α are also found along the equatorial Atlantic and the tropical Indian Ocean. In the 20C simulation τ_m is smaller above the Atlantic and the Indian Ocean in comparison with the ERA-40 data. In the extra-tropics memory is present over all ocean basins and continents with varying extent towards the Polar Regions. The main differences between the different time scales are visible in their zonal means. In general the zonal mean reveals a maximum at the equator and additional much less pronounced peaks at 60° latitude. The longer the time period considered in the

analysis, the stronger the North–South gradient at the equator.

The global memory distributions of CIN reveal similarities to those of CAPE, which is surprising as the global distribution of CIN itself was found to differ quite strongly to that of CAPE (Riemann-Campe *et al.*, 2009). The highest values of τ_m and α in CIN occur along the equator but are less pronounced regarding spatial extent and strength compared to CAPE. However, the highest τ_d values in CIN occur over the Indian Ocean, North and South of the tropical Atlantic, and the tropical Pacific. Furthermore, the distributions of smaller values of τ_d , τ_m and α reveal stronger similarities between τ_m and α . CAPE and CIN display similar distributions of decay time scales and Hurst exponents, which demonstrates CIN memory in almost all regions.

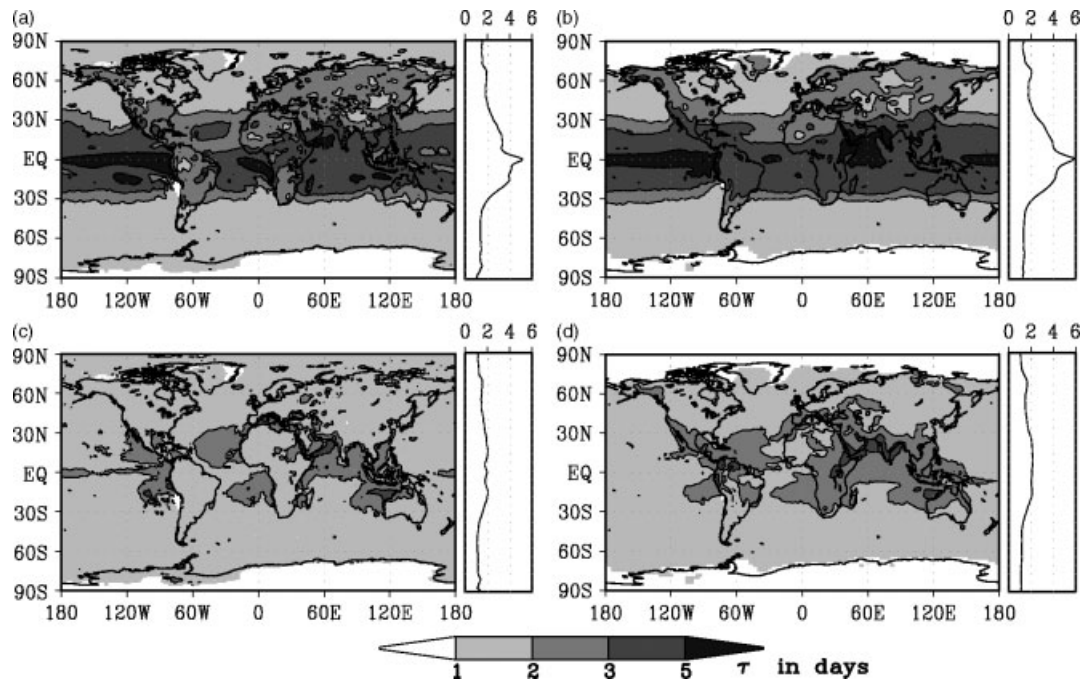


Figure 4. Decay time scale τ_d in days of CAPE (a and b) and CIN (c and d) computed from ERA-40 data (1979–2001) (a and c) and the 20C simulation (1900–2001) (b and d).

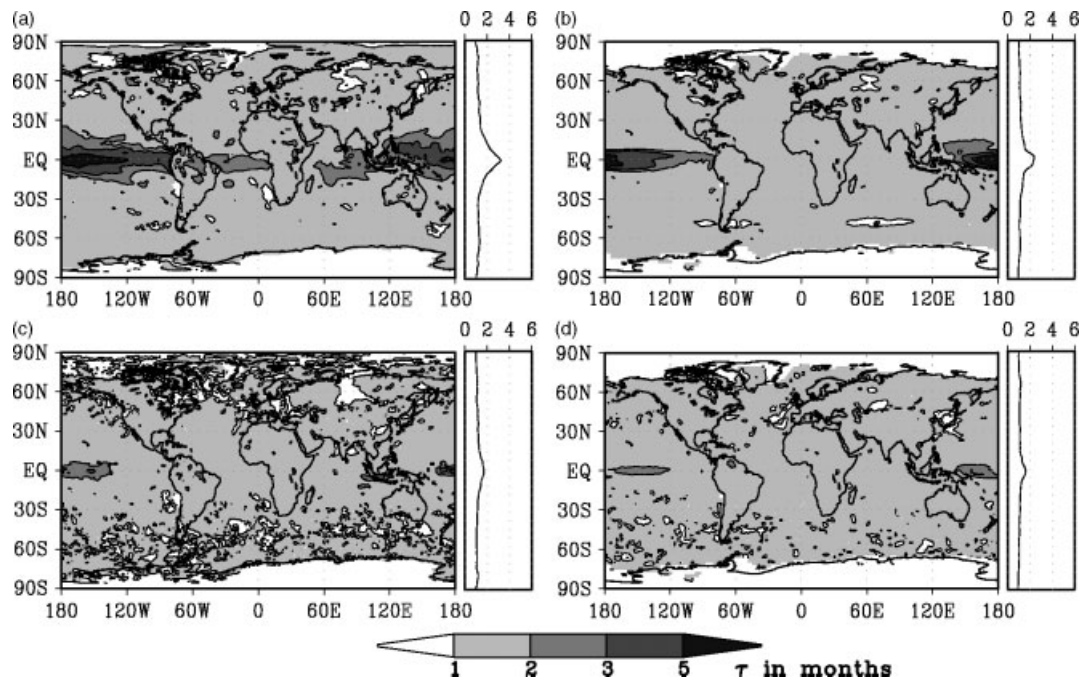


Figure 5. Decay time scale τ_m in months of CAPE (a and b) and CIN (c and d) computed from ERA-40 data (1979–2001) (a and c) and the 20C simulation (1900–2001) (b and d).

5.2. Inter-annual memory

The global distribution of inter-annual memory is determined by the Hurst exponent α in the time interval of 400 days to 5 years (Figure 7). The general pattern of the inter-annual memory distribution in CAPE resembles those of intra-annual memory. Highest values of $\alpha \geq 1$ occur over the equatorial Pacific. The Hurst exponent reaches up to $\alpha = 1.4$ over central and western parts

of the Pacific. Such high values are caused by ENSO (see Subsection 4.1). The ENSO cycle, which superimposes the memory signal, enlarges the Hurst exponent in the periodicities affected (between 1000 and 2000 days). In the 20C simulation the regions with $\alpha > 1$ show a larger spatial extent. According to van Oldenborgh *et al.* (2005) the ENSO cycle is represented realistically regarding its strength and location within the 20C simulation. Therefore, the smaller Hurst exponent indicates an

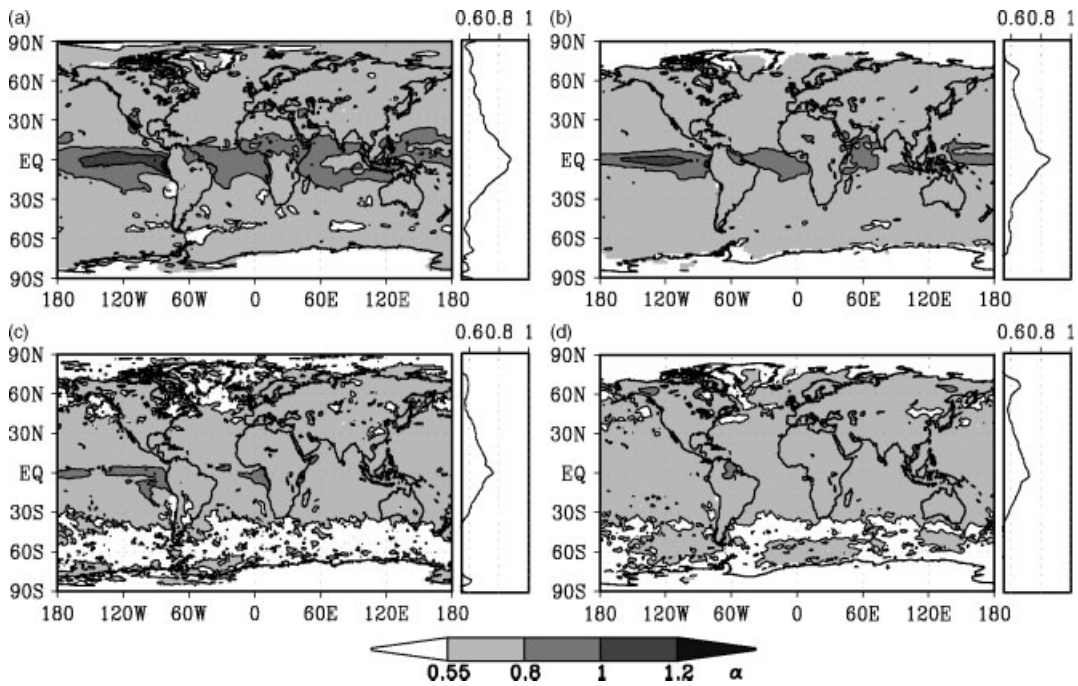


Figure 6. Hurst exponent α of CAPE (a and b) and CIN (c and d) computed from ERA-40 data (1979–2001) (a and c) and the 20C simulation (1900–2001) (b and d): Global distribution and zonal mean for 30–300 days. Hurst exponents exceeding 0.55 indicate memory.

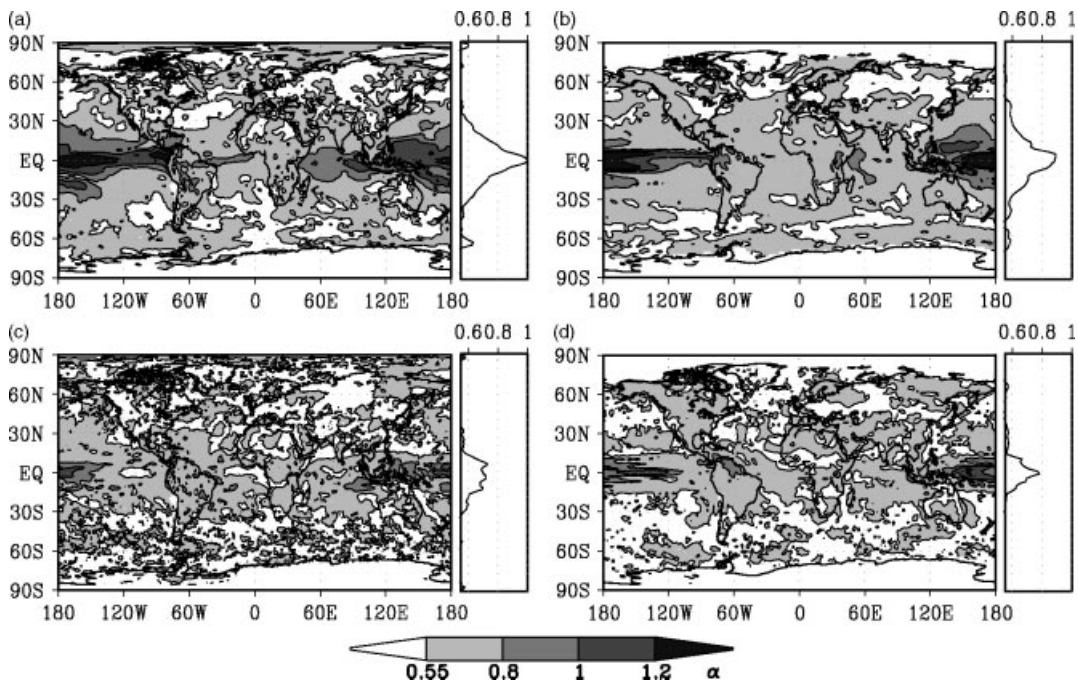


Figure 7. Hurst exponent α of CAPE (a and b) and CIN (c and d) computed from ERA-40 data (1979–2001) (a and c) and the 20C simulation (1900–2001) (b and d): Global distribution and zonal mean for 400 days to 5 years. Hurst exponents exceeding 0.55 indicate memory.

underestimation of ENSO in the ERA-40 data which is probably related to the shorter length of data set. In the tropics high α -values are also present over the equatorial Atlantic and Indian Ocean in the ERA-40 data, whereas they only occur over the tropical Indian Ocean in the 20C simulation. Memory occurs in the extra-tropics over the continents with the exception of Antarctica and Greenland. Furthermore, memory is present over all oceans including the polar oceans. The zonal mean emphasises

the ENSO cycle which leads to a strong gradient towards the equator.

The memory visible over the polar oceans is related to the variability in polar low occurrence. Claud *et al.* (2007) report associations between large-scale atmospheric circulations and polar low development over the North Atlantic including SST distribution, sea ice extent and the NAO. Carleton and Carpenter (1990) report similar relations for the Southern Hemisphere. According to

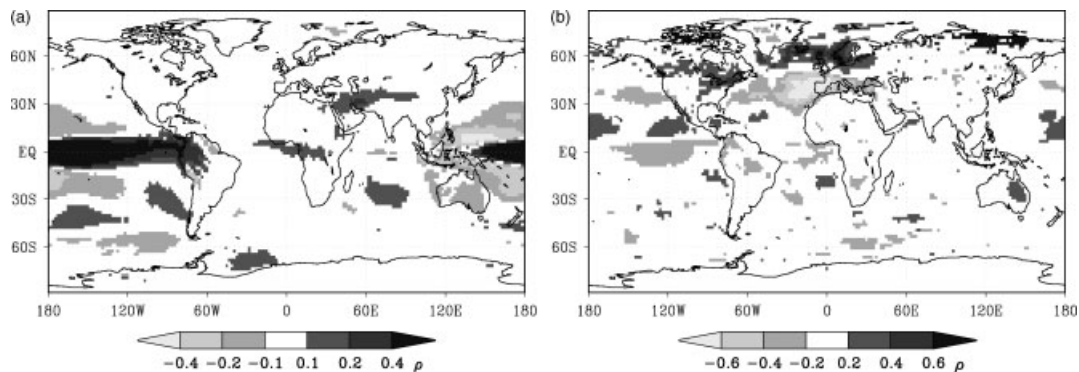


Figure 8. Correlations between CAPE and ENSO (a), and CAPE and NAO (b). Correlation coefficients ρ computed from monthly means of the 20C simulation: 1900–2001. Grey shadings are significant at the 95% level.

their studies polar low occurrences and thus CAPE are related to sea ice extent and ENSO.

The global distribution of α in CIN reveals similarities to that of CAPE. Again, this is a surprising result as the global distribution of CIN itself was found to differ quite strongly to that of CAPE (Riemann-Campe *et al.*, 2009). The highest values of α in CIN occur along the equatorial Pacific but are less pronounced regarding spatial extent and strength compared to CAPE. This suggests that ENSO also influences the memory in CIN. However, ENSO is only visible in the 20C simulation. Memory in CIN is also visible in many other tropical and extra-tropical regions similar to the distribution in CAPE.

6. Correlations between ENSO, NAO and CAPE

ENSO is clearly visible in CAPE in global and regional memory analysis in the 20C simulation. The long memory in CAPE over the North Atlantic in both datasets suggests a relation between NAO and CAPE. To confirm these relations a spearman rank correlation is applied on CAPE with ENSO and NAO which are determined by SST, and mean sea level pressure (MSLP) respectively. Correlations are based on monthly mean values from the 20C simulation during 1900–2001. The 95% significance level is estimated by Fisher's z-transformed inferences. The ENSO time series is determined from the field mean of a 5-month running mean of SST anomalies within the Niño 3 region (150°W–90°W; 5°S–5°N) (Trenberth, 1997). The NAO-index time series consists of the first principal component computed via Empirical Orthogonal Functions applied to the anomalies of MSLP mean winter months (December, January, February) in the North Atlantic sector (90°W–40°E; 20°–70°N) (Hurrell and Deser, 2010).

The correlation between ENSO and CAPE (Figure 8(a)) reveals the typical pattern of a positive relationship along the equatorial Pacific and a negative relationship along 20° North and South, respectively, in the eastern Pacific. Furthermore, a positive correlation exists above the eastern equatorial Atlantic.

The correlation between NAO-index and CAPE (Figure 8(b)) shows first the typical dipole pattern in the

North Atlantic and second additional teleconnections in the tropical Pacific with ENSO and in the northern Pacific with the Pacific North America pattern. These findings support the ENSO-Europe link (Fraedrich, 1994) with ENSO displacing the tail end of the cross Atlantic storm track with its frontal systems, whose locations affect the spatial distribution of CAPE. The correlation between NAO and ENSO is present except in Figure 8(b), as the strongest NAO signal occurs during winter and is too weak to be visible in a correlation based on the annual anomalies (Figure 8(a)).

7. Discussion and conclusions

The comparisons of ERA-40 data with the 20C simulation revealed a good agreement of the global memory patterns. The strongest memory signals in CAPE and CIN occurred along the equatorial Pacific, caused by the ENSO cycle. A general strong memory in CAPE was visible on inter-annual time scales in the tropics, extending to extra-tropical regions on all continents except Antarctica, and over all oceans including the polar oceans. The memory in CAPE and CIN lasts up to 9000 days south-east of Greenland.

The memory analysis of related parameters (T_{ML} , q_{ML} , H , and LPW) revealed that their influence on memory in CAPE and CIN differs with location. In the tropics, the spatial pattern in LPW resembled that of CAPE suggesting that it plays the dominant role in CAPE memory. These findings are confirmed by the study of Holloway and Neelin (2009), who reported a correlation between buoyancy and specific humidity in the free troposphere over the tropical Pacific. However, in our study, the extra-tropical T_{ML} and q_{ML} had a stronger influence on the memory of CAPE when comparing their spatial memory patterns.

Polar low occurrence yields an explanation on probable mechanisms of the STM and LTM for CAPE found in the Polar Regions, as considerable CAPE is accumulated in polar lows. On the one hand, STM up to three days represents the duration of a polar low life cycle. On the other hand, LTM may be caused by the correlation we found between CAPE and the NAO. Similar relations

were reported by Claud *et al.* (2007), substantiating our findings concerning the NAO. Correlations between monthly means of CAPE and NAO, as well as ENSO, revealed global teleconnections. Consequently, ENSO was identified to influence strongly the variability in CAPE and CIN in the tropical Pacific.

Almost all continents and ocean basins show memory in daily CAPE and CIN time series at long time scales. This should help to improve predictability of deep convection. In regions where $1/f$ scaling occurs in CAPE within certain time scales, the analysis of temporal trends and extreme event recurrence times requires a careful provision for the non-stationarity.

This study focused on the memory during the 20th century. The question arises how the memory will change during the coming decades and how it will influence future trends. Memory changes in future scenarios may be expected considering the atmospheric cycles presented here.

Acknowledgements

We acknowledge most helpful discussions with Nikolai Dotzek and Frank Lunkeit, computational help by Frank Sielmann, the DKRZ, DWD, and ECMWF for providing the data, and support by IMPRS-ESM (for K. R.-C.).

References

- Bengtsson L, Hagemann S, Hodges KI. 2004. Can climate trends be calculated from reanalysis data?. *Journal of Geophysical Research* **109**: D11111, DOI: 10.1029/2004JD004536.
- Blender R, Fraedrich K. 2003. Long time memory in global warming simulations. *Geophysical Research Letters* **30**: 1769–1772, DOI: 10.1029/2003GL017666.
- Brooks HE, Anderson AR, Riemann K, Ebberts I, Flachs H. 2007. Climatological aspects of convective parameters from the NCAR/NCEP reanalysis. *Atmospheric Research* **83**: 294–305, DOI: 10.1016/j.atmosres.2005.08.005.
- Brooks HE, Lee JW, Craven JP. 2003. The spatial distribution of severe thunderstorm and tornado environments from global reanalysis data. *Atmospheric Research* **67–68**: 73–94, DOI: 10.1016/S0169-8095(03)00045-0.
- Carleton AM, Carpenter DA. 1990. Satellite climatology of 'polar lows' and broadscale climatic associations for the Southern Hemisphere. *International Journal of Climatology* **10**: 219–246, DOI: 10.1002/joc.3370100302.
- Claud C, Duchiron B, Terray P. 2007. Associations between large-scale atmospheric circulation and polar low developments over the North Atlantic during winter. *Journal of Geophysical Research* **112**: D12101, DOI: 10.1029/2006JD008251.
- Colby JRFP. 1984. Convective inhibition as a predictor of convection during AVE-SESAME II. *Monthly Weather Review* **112**: 2239–2252, DOI: 10.1175/1520-0492(1984)112<2239:CLAAPO>2.0.CO;2.
- Craven JP, Brooks HE, Hart JA. 2002. Baseline climatology of sounding derived parameters associated with deep moist convection. *National Weather Digest* **28**: 13–24.
- Doswell CA III, Evans JS. 2003. Proximity sounding analysis for derechos and supercells: an assessment of similarities and differences. *Atmospheric Research* **67–68**: 117–133, DOI: 10.1016/S0169-8095(03)00047-4.
- Emanuel KA. 1994. *Atmospheric Convection*. Oxford University Press: Oxford.
- Fraedrich K. 1994. An ENSO impact on Europe? A review. *Tellus A* **46**: 541–552, DOI: 10.1034/j.1600-0870.1994.00015.x.
- Fraedrich K. 2002. Fickian diffusion and Newtonian cooling: a concept for noise induced climate variability with long-term memory?. *Stochastics and Dynamics* **2**: 403–412.
- Fraedrich K, Blender R. 2003. Scaling of atmosphere and ocean temperature correlations in observations and climate models. *Physical Review Letters* **90**: 108501, DOI: 10.1103/PhysRevLett.90.108501.
- Fraedrich K, Larnder C. 1993. Scaling regimes of composite rainfall time series. *Tellus* **45A**: 289–298.
- Fraedrich K, Luksch U, Blender R. 2004. $1/f$ model for long-time memory of the ocean surface temperature. *Physical Review E* **70**: 037301, DOI: 10.1103/PhysRevE.70.037301.
- Holloway CE, Neelin JD. 2009. Moisture vertical structure, column water vapor, and tropical deep convection. *Journal of the Atmospheric Sciences* **66**: 1665–1683, DOI: 10.1175/2008JAS2806.1.
- Hurrell JW, Deser C. 2010. North Atlantic climate variability: the role of the North Atlantic Oscillation. *Journal of Marine Systems* **79**: 231–244, DOI: 10.1016/j.jmarsys.2008.11.026.
- Maraun D, Rust HW, Timmer J. 2004. Tempting long-memory—on the interpretation of DFA results. *Nonlinear Processes in Geophysics* **11**: 495–503.
- Margules M. 1905. *Über die Energie der Stürme*. Jahrbuch der K. K. Zentralanstalt für Meteorologie: Wien.
- Markowski PM, Straka JM, Rasmussen EN. 2002. Direct surface thermodynamic observations within rearflank downdrafts of nontornadic and tornadic supercells. *Monthly Weather Review* **130**: 1692–1721, DOI: 10.1175/1520-0493(2002)130<1692:DSTOWT>2.0.CO;2.
- Moncrieff MW, Miller M. 1976. The dynamics and simulation of tropical cumulonimbus and squall lines. *The Quarterly Journal of the Royal Meteorological Society* **102**: 373–394, DOI: 10.1002/qj.49710243208.
- van Oldenborgh GJ, Philip SY, Collins M. 2005. El Niño in a changing climate: a multi-model study. *Ocean Science* **1**: 81–95.
- Peng C-K, Havlin S, Stanley HE, Goldberger AL. 1995. Quantification of scaling exponents and crossover phenomena in nonstationary heartbeat time series. *Chaos* **5**: 82, DOI:10.1063/1.166141.
- Rasmussen EN, Blanchard DO. 1998. A baseline climatology of sounding-derived supercell and tornado forecast parameters. *Weather and Forecasting* **13**: 1148–1164, DOI: 10.1175/1520-0434(1998)013<1148:ABCOSD>2.0.CO;2.
- Riemann-Campe K, Fraedrich K, Lunkeit F. 2009. Global climatology of convective available potential energy (CAPE) and convective inhibition (CIN) in ERA-40 reanalysis. *Atmospheric Research* **93**: 534–545, DOI: 10.1016/j.atmosres.2008.09.037.
- Roeckner E, Bäuml G, Bonaventura L, Brokopf R, Esch M, Giorgetta M, Hagemann S, Kirchner I, Kornbluh L, Manzini E, Rhodin A, Schlese U, Schulzweida U, Tompkins A. 2003. The atmospheric general circulation model ECHAM5 part I model description. Max-Planck-Institut für Meteorologie, Report No. 349, Hamburg.
- Simmons AJ, Jones PD, da Costa Bechtold V, Beljaars ACM, Kållberg PW, Saarinen S, Uppala SM, Viterbo P, Wedi N. 2004. Comparison of trends and low-frequency variability in CRU, ERA-40, and NCEP/NCAR analyses of surface air temperature. *Journal of Geophysical Research* **109**: D24115, DOI: 10.1029/2004JD005306.
- Trapp RJ, Diffenbaugh NS, Brooks HE, Baldwin ME, Robinson ED, Pal JS. 2007. Changes in severe thunderstorm environment frequency during the 21st century caused by anthropogenically enhanced global radiative forcing. *Proceedings of the National Academy of Sciences of the United States of America* **104**: 19719–19723, DOI: 10.1073/pnas.0705494104.
- Trapp RJ, Diffenbaugh NS, Gluhovsky A. 2009. Transient response of severe thunderstorm forcing to elevated greenhouse gas concentrations. *Geophysical Research Letters* **36**: L01703, DOI: 10.1029/2008GL036203.
- Trenberth KE. 1997. The definition of El Niño. *Bulletin of the American Meteorological Society* **78**: 2771–2777, DOI: 10.1175/1520-0477(1997)078<2771:TDOENO>2.0.CO;2.
- Vyushin DI, Kushner PJ. 2009. Power-law and long-memory characteristics of the atmospheric general circulation. *Journal of Climate* **22**: 2890–2904, DOI: 10.1175/2008JCLI2528.1.
- Washington WM, Parkinson CL. 2005. *An Introduction to Three-Dimensional Climate Modeling*. University Science Books: United States of America.
- Yano J-I, Fraedrich K, Blender R. 2001. Tropical convective variability as $1/f$ noise. *Journal of Climate* **14**: 3608–3616, DOI: 10.1175/1520-0442(2001)014<3608:TCVAFN>2.0.CO;2.
- Ye B, Del Genio AD, Lo KK-W. 1998. CAPE variations in the current climate and in a climate change. *Journal of Climate* **11**: 1997–2015, DOI: 10.1175/1520-0442(1998)011<1997:CVITHCC>2.0.CO;2.